

## Research Paper

# Enhanced Therapeutic Effect of RGD-Modified Polymeric Micelles Loaded With Low-Dose Methotrexate and Nimesulide on Rheumatoid Arthritis

Yunlong Wang<sup>1,2\*</sup>, Zhongbing Liu<sup>1\*</sup>, Ting Li<sup>\*</sup>, Lin Chen<sup>1\*</sup>, Jiayao Lyu<sup>1</sup>, Chunhong Li<sup>1</sup>, Yan Lin<sup>1</sup>, Na Hao<sup>1</sup>, Meiling Zhou<sup>4</sup>, Zhirong Zhong<sup>1,3</sup>

1. Department of Pharmaceutical Sciences, School of Pharmacy, Southwest Medical University, Luzhou 646000, China
2. Department of Pharmacy, Nanchong Central Hospital, The Second Clinical Medical College of North Sichuan Medical College, Nanchong 637000, China
3. Key Laboratory of Medical Electrophysiology, Ministry of Education, Institute of Cardiovascular Research of Southwest Medical University, Luzhou 646000, China.
4. Department of Pharmacy, the Affiliated Hospital of Southwest Medical University, Luzhou 646000, China

\*These authors contributed equally to this work.

 Corresponding authors: Dr. Meiling Zhou: Tel./fax 8618084955975 and E-mail meilzhou@163.com; Dr. Zhirong Zhong: Tel./fax +8613982796280 and E-mail zhongzr@swmu.edu.cn.

© Ivyspring International Publisher. This is an open access article distributed under the terms of the Creative Commons Attribution (CC BY-NC) license (<https://creativecommons.org/licenses/by-nc/4.0/>). See <http://ivyspring.com/terms> for full terms and conditions.

Received: 2018.10.04; Accepted: 2018.12.24; Published: 2019.01.24

## Abstract

Angiogenesis plays an essential role in the progression of rheumatoid arthritis (RA). RGD peptide shows high affinity and selectivity for integrin  $\alpha_v\beta_3$ , which is one of the most extensively examined target of angiogenesis. Nimesulide could improve the anti-rheumatic profile of methotrexate. But the clinical application was limited due to water-insolubility of both methotrexate and nimesulide and lacking targeting ability. Therefore, this study aimed to design a targeted drug delivery system of micelles mediated by RGD plus the passive targeting of micelles to solve the application problems of methotrexate and nimesulide (M/N), and thus enhance their combined therapeutic effect on RA.

**Methods:** RGD was conjugated with NHS-PEG-PLA to form RGD-PEG-PLA for the preparation of RGD-modified drug-loaded micelles (R-M/N-PMs). The size and zeta potential of micelles were measured by dynamic light scattering. Morphology was detected by transmission electron microscopy. The inhibition effect of R-M/N-PMs on angiogenesis was assessed by the chick chorioallantoic membrane assay. The real-time fluorescence imaging analysis was conducted to examine the *in vivo* distribution of the fluorescence-labeled R-M/N-PMs. Rats arthritis model induced by Freund's adjuvant was used to evaluate the *in vivo* anti-inflammatory efficacy of R-M/N-PMs.

**Results:** The *in vitro* study indicated successful development of R-M/N-PMs. R-M/N-PMs could markedly suppress the angiogenesis of chick embryos. The fluorescence-labeled R-M/N-PMs mainly accumulated in arthritic joints. RGD enhanced the targeting ability of micelles and thus promoted retention of micelles in arthritic joints. Moreover, R-M/N-PMs significantly alleviated the joint swelling while reducing bone erosion and serum levels of inflammatory cytokines. It helped to recover the bone microstructure of arthritic rats.

**Conclusion:** Our results confirmed that the targeted delivery of the combination of a low dose of methotrexate and nimesulide mediated by RGD-modified polymeric micelles could enhance the therapeutic effect on rheumatoid arthritis. These findings provide a promising potential for the clinical therapy of rheumatoid arthritis.

Key words: RGD; Polymeric micelles; Methotrexate; Nimesulide; Rheumatoid arthritis

## Introduction

Rheumatoid arthritis (RA), a chronic auto-immune disease, is characterized by infiltration of inflammatory mononuclear cells, excessive synovial

hyperplasia, pannus formation over the joint surface and progressive joint destruction [1]. At present, there is no cure for RA because of its complex etiology and

multifactorial pathogenesis [2, 3]. Current strategies for the treatment of RA include disease-modifying anti-rheumatic drugs (DMARDs), non-steroidal anti-inflammatory drugs (NSAIDs), glucocorticoids (GC), and novel biologics like TNF $\alpha$ -blocking agents [4, 5] and B-cell targeted therapy [6]. However, because of the high cost of novel biologics and the severe side effects of glucocorticoids, the conventional DMARDs are still widely used in clinical therapy [7]. According to the guidelines of the American College of Rheumatology, newly diagnosed RA patients receive NSAIDs for reducing acute pain and suppressing inflammation in combination with DMARDs for relieving disease activity and preventing joint damage [8]. Methotrexate (MTX), which is a chemotherapy drug and an immunosuppressant, is one of the most commonly used DMARDs for the treatment of RA [9-11]. However, MTX was reported to cause significant systemic toxicity, especially for highly proliferative cells in the gastrointestinal mucosa and bone marrow. Nimesulide (NIM), which belongs to the NSAID class of drugs and is a COX-2 inhibitor, is widely used for symptomatic alleviation of RA [12]. The combined application of MTX and NIM for RA was suggested to increase therapeutic efficacy and minimize the side effects of MTX [13]. However, some disadvantages like poor water-solubility of both MTX and NIM and poor pharmacokinetics and narrow safety dose of MTX limit their application in the treatment of various diseases. Moreover, both MTX and NIM lack tissue specificity, which leads to serious side effects including reproductive toxicity, gastrointestinal lesions, and cardiovascular complications. Therefore, nanotherapeutics and the targeted delivery strategies for improving the target tissue accumulation of drugs have attracted considerable attention in recent years for the treatment of RA [14-16].

It has been reported that the polymeric micelles, as nano-sized drug carriers, show various advantages such as prolonging the circulation time in blood, improving the solubility of hydrophobic drugs, controlling the drug release pattern, and protecting the cargos from degradation *in vivo* [17, 18]. Therefore, polymeric micelles are considered ideal carriers for specific drugs with low solubility and side effects such as MTX and NIM. More importantly, polymeric micelles may be passively targeted to sites of inflammation according to the ELVIS (Extravasation through Leaky Vasculature and Inflammatory cell-mediated Sequestration) mechanism [19].

Inflammation and angiogenesis are two crucial factors in the initiation and persistence of arthritic disease and targeting both features may yield effective therapeutic strategies for successfully treating RA [20]. RGD peptide is known to have an

affinity for  $\alpha_v\beta_3$  integrin that is over-expressed on angiogenic endothelial cells [21]. We hypothesized that RGD-mediated polymeric micelles loaded with low-dose methotrexate and nimesulide, would drive both passive and active targeting, and enhance the combined therapeutic effect of both drugs on rheumatoid arthritis. We, therefore, conjugated RGD onto an amphiphilic copolymer of NHS-PEG<sub>3400</sub>-PLA<sub>2000</sub>, one of the biocompatible and biodegradable materials approved by FDA [22, 23], to form RGD-PEG<sub>3400</sub>-PLA<sub>2000</sub>. Subsequently, we prepared RGD-modified drug-loaded micelles (R-MTX-PMs, R-NIM-PMs) by the filming-rehydration method in which the combination of R-MTX-PMs and R-NIM-PMs was designated as R-M/N-PMs. We assessed the toxicity of micelles by the *in vitro* hemolysis test and detected the inhibitory effect of R-M/N-PMs on angiogenesis using the chick chorioallantoic membrane assay. Furthermore, we conducted the real-time fluorescence imaging analysis to examine the *in vivo* distribution of the fluorescence-labeled R-M/N-PMs and performed *in vivo* studies in a rat model with adjuvant-induced arthritis to assess the anti-inflammatory efficacy of R-M/N-PMs.

## Materials and Methods

### Materials

Methotrexate was supplied by the National Institutes for Food and Drug Control (Beijing, China). Nimesulide was obtained from Tokyo Chemical Industry Corporation (Tokyo, Japan; purity >98%). mPEG<sub>3400</sub>-PLA<sub>2000</sub> and NHS-PEG<sub>3400</sub>-PLA<sub>2000</sub> polymer were purchased from Xi'an Ruixi Biotechnology Company (Xi'an, China). RGD tri-peptide was obtained from Nanjing Peptide Biotech Company (Nanjing, China; purity >95%). Methanol and acetonitrile (HPLC grade) were purchased from Kelong Chemical Reagent Factory (Chengdu, China). Complete Freund's adjuvant (CFA) was acquired from Chondrex (Washington DC, USA). ELISA kits were from Shanghai Qiaodu Biotechnology Company (Shanghai, China).

### Cell lines and animals

The murine macrophage cell line Raw264.7 and human umbilical vein endothelial cell line (HUVEC) were purchased from the Shanghai Cell Institute, China Academy of Sciences, and preserved in our laboratory. Dulbecco's Modified Eagle's Medium (DMEM) and fetal bovine serum (FBS) were obtained from Gibco Laboratories (Grand Island, NY, USA). 3-(4,5 dimethylthiazol-2-yl)-2,5-diphenyl-tetrazolium bromide (MTT) and dimethyl sulfoxide (DMSO) were purchased from Sigma (USA). Paraformaldehyde was

provided by Jinshan Chemical Company (Chengdu, China). Both Raw264.7 and HUVEC cells were cultured in DMEM containing 10% FBS, 100 U/mL penicillin and 100 mg/mL streptomycin at 37 °C with 5% CO<sub>2</sub>.

Male Sprague-Dawley rats (160 ± 20 g) were supplied by the Experimental Animal Center of Southwest Medical University (Lu zhou, China). The rats were maintained under standardized conditions. All animal tests were approved by the Institutional Animal Care and Ethics Committee of Southwest Medical University (permit No. 2017050009).

### Preparation of RGD-modified micelles loaded with MTX and NIM

To prepare the RGD-modified micelles loaded with MTX and NIM, we first synthesized the copolymer RGD-PEG<sub>3400</sub>-PLA<sub>2000</sub> as shown in **Figure 1A**, using NHS-PEG<sub>3400</sub>-PLA<sub>2000</sub> as a crosslinker as described previously [22]. Briefly, 130 mg of NHS-PEG<sub>3400</sub>-PLA<sub>2000</sub> was dissolved in anhydrous N, N-dimethyl formamide (DMF) and mixed with 25 µL of anhydrous triethylamine (TEA). Subsequently, 10 mg of RGD was added to the mixture, stirred at room temperature for 24 h and then dialyzed (MWCO 3,500 Da) against deionized water for 48 h to remove the unconjugated RGD. The solution was immediately lyophilized after dialysis and subjected to <sup>1</sup>H NMR (400 MHz, DMSO-d<sub>6</sub>) detection to confirm the conjugation of RGD with PEG<sub>3400</sub>-PLA<sub>2000</sub>.

Polymeric micelles were prepared by the filming-rehydration method according to the published literature with minor modification [22, 23]. In brief, the preformed RGD-PEG<sub>3400</sub>-PLA<sub>2000</sub> copolymer (40 mg) and MTX/NIM (4 mg) were dissolved in 2 mL DMF. The mixture was dried under reduced pressure at 50 °C until a dry thin-film formed. To remove any residual DMF, it was maintained in a vacuum drying chamber for overnight at room temperature. Then, 2 mL saline was added and kept in an incubator at 37 °C with slow shaking for 1 h. Subsequently, the solution was ultrasonicated for 15 min at 25 °C. Finally, the micelles solution was centrifuged at 15,000 × g for 10 min to remove the unloaded drugs. The blank micelles (PMs) and RGD-free micelles were also prepared according to the described procedure.

### Characterization of micelles

The size and zeta potential of micelles including PMs, MTX-PMs, NIM-PMs, R-MTX-PMs and R-NIM-PMs were measured by the dynamic light scattering (DLS) method using a Malvern Zetasizer Nano ZS90 (Malvern Instruments, U.K.). Morphology of micelles was observed by transmission electron

microscopy (TEM). Critical micelle concentration (CMC) was measured by a fluorescence technique using pyrene as the fluorescence probe as described previously [24]. Encapsulation efficiency (EE) and drug loading (DL) of micelles were measured using high-performance liquid chromatography (HPLC). Measurements were performed on an Agilent ZORBAX Eclipse XDB-C18 column (5 µm, 150 × 4.6 mm). For the detection of MTX, the flow phase was prepared with a mixture of sodium dihydrogen phosphate (10 mmol/L) and methanol (26:74, v/v). The detection wavelength was 302 nm, which corresponds to the maximum absorption of MTX. In case of NIM, the flow phase was the mixture of 0.1% phosphoric acid (pH 7.0) and acetonitrile (60:40, v/v) and the detector was set to monitor the signal at 295 nm. All measurements were conducted at 25 °C with a flow rate of 1.0 mL/min and an injection volume of 20 µL. The selectivity, linearity, precision, and recovery of methods were fully validated. Encapsulation efficiency and drug loading were determined using the following formulae:

$$EE (\%) = (\text{Weight of the drug encapsulated in micelles}) / (\text{Weight of the total drug}) \times 100\%$$

$$DL (\%) = (\text{Weight of the drug encapsulated in micelles}) / (\text{Weight of the total micelles}) \times 100\%$$

### In vitro release of MTX and NIM from micelles

*In vitro* release of micelles including MTX-PMs, NIM-PMs, R-MTX-PMs, and R-NIM-PMs were investigated using the dialysis method with PBS with 1% Tween-80 as the release medium. Briefly, three batches of the preformed micelles were added into dialysis bags with a molecular weight cut-off of 3.5 kDa (Millipore) and placed in 50 mL of release medium. The whole device was placed in a water bath at 37 °C for 96 h. At the pre-designed time points of 0.5, 1, 2, 4, 6, 8, 12, 24, 36, 48, 72 and 96 h, 2.0 mL of the solution from the release medium was taken and replaced with fresh medium. The sample was brought up to 5 mL with methanol and filtered through a 0.22-µm membrane (Millipore). The concentrations of MTX or NIM in various micelles were determined by the HPLC method described above.

### Toxicity assay of micelles by in vitro hemolysis

Rat red blood cells (RBCs) were collected to evaluate the hemolytic potential of MTX/NIM-loading micelles. RBCs were centrifuged 5 times at 2,000 × g for 8 min and suspended in 10 mL of saline. 500 µL of different concentrations (5.65, 56.5, 565 µg/mL) of MTX-PMs, NIM-PMs, M/N-PMs (MTX-PMs + MIN-PMs), and R-M/N-PMs (R-MTX-PMs + R-MIN-PMs) were incubated with 500 µL of RBCs suspension (2%) with normal saline and cell

lysis solution (RIPA) as negative and positive controls, respectively [25]. After incubation at 37 °C for 3 h, the samples were centrifuged at 2,500 g for 10 min. 150 µL of the supernatants were collected and placed into 96-well plates to analyze the hemoglobin content by microplate reader at 540 nm. The hemolysis rate (%) was calculated according to the following formula:

$$\text{Hemolysis rate (\%)} = \frac{(A_{\text{sample}} - A_{\text{negative control}})}{(A_{\text{positive control}} - A_{\text{negative control}})} \times 100\%.$$

### Chick chorioallantoic membrane assay

The chick chorioallantoic membrane (CAM) assay was conducted to analyze the anti-angiogenic activity of micelles formulation [21, 26, 27]. Chicken eggs were fertilized and incubated at 37 °C with a relative humidity of 60%. On day 6, all eggs were swabbed with ethanol solution (75%). A small hole was made at the end of the chamber with a hypodermic needle. The second hole was made in the center of the egg which was directly located over the avascular portion of the embryonic membrane. By using a negative pressure through the first hole to separate CAM from the shell, a false air chamber was created. After an additional incubation for 48 h, a 1.0-cm-diameter window was made with an embroidery needle and a tweezer, and the shell membrane was peeled away. Sterile filter papers (about 6 mm<sup>2</sup>), pretreated with saline as control and PMs, MTX-PMs, NIM-PMs, M/N-PMs, R-MTX-PMs, R-NIM-PMs, R-M/N-PMs, were placed on the vessels surface and air-dried under sterile conditions. After incubating for 24 h, the area around the filter paper was peeled off and photographed using a Canon digital camera.

### Construction of the arthritis model induced by CFA

We used CFA to induce arthritis in the rats. Briefly, 0.12 mL of CFA that contained 10 mg/mL of heat-killed mycobacteria was subcutaneously injected at the base of the rat tail [11, 28] using saline injection as a control. During disease progression, all rats could freely access sterile food and water. The arthritis progression was monitored daily.

### Distribution of R-M/N-PMs in arthritic rats

Following the intravenous injection in SD rats with arthritis, the distribution of micelles was investigated by the *in vivo* small animal imaging system (Bruker, Fx Pro/FX, USA). DiD (KeyGEN BioTECH), a hydrophobic infrared fluorescent dye, was used as the tracer (5 µg DiD per rat) in free form or encapsulated into polymeric micelles [14]. Arthritic rats with whole body hair removed by depilation

cream were randomly divided into four groups (n=3) of saline, DiD, M/N-PMs-DiD, and R-M/N-PMs-DiD. Each rat received an intravenous injection of 0.2 mL of different micelle solutions, in which the MTX and NIM dose was 0.6 mg/kg and 3.0 mg/kg, respectively, as determined by our preliminary experiments and according to a published report [13]. The rats were anesthetized at the designated time points (3 h, 16 h, and 24 h) and visualized in imaging systems, in which the filters for excitation and emission were set at 644 nm and 665 nm, respectively, to measure fluorescence intensity of DiD. The images of each rat used the same intensity scale with the same range of minimum and maximum values. The fluorescence intensity was quantified using NIH Image-Pro Plus 6.0.

### Measurement of weight, ankle diameter, and articular index score in arthritic rats

After injection with CFA to induce arthritis, the diet, mental state, fur color, walking gait, and joint swelling of the rats were observed every day. The weight of each rat was measured every other day during the disease progression from day 0. On day 19 post-induction, arthritis in rats was at the peak level, showing severe swelling and erythema in limbs, especially the hind limbs. Arthritic rats were randomly assigned to eight groups (n = 5) and injected intravenously with 0.2 mL of saline, PMs, MTX-PMs, NIM-PMs, M/N-PMs, R-MTX-PMs, R-NIM-PMs and R-M/N-PMs on days 19, 21, 23, and 25 after arthritis induction, in which the MTX dose was 0.6 mg/kg and the NIM dose was 3.0 mg/kg. The normal healthy rats were injected with equal volume of saline as control. The ankle diameter from medial to lateral of each rat was detected every other day using a digital caliper. The articular index (AI) score in each limb of all animals was assessed from day 19 to day 27 post-arthritis inductions following a previously described method with minor modifications [29]. In brief, the AI scoring was made according to a numeric system with a score ranging from 0 to 4, in which the absence of swelling or erythema was considered to be 0; a mild swelling and/or erythema was 1; a moderate edema and signs involving the tarsals was 2; a visible edema with limited use of the joint and signs extending to the metatarsals was 3; and an excessive edema with joint rigidity and severe signs involving the entire paw was 4. The final arthritis score of each rat was the sum of the two hind limb scores.

### Micro-computed tomography analysis of ankle joints

On day 27 after induction, rats of each group (n = 5) were euthanized and the left ankle joints were fixed

by 10% neutral buffered formalin for 48 h to evaluate the bone density of ankle joints using a high-resolution Micro-computed tomography (Micro-CT, SIEMENS healthcare, Berlin and Munich Germany) [11, 30]. Parameters of Micro-CT scanning were set as voltage 55 kV, current 189  $\mu$ A, exposure time 230 ms, resolution 6.2  $\mu$ m and aluminum filter 0.5 mm. The three-dimensional (3D) reconstruction was performed for visualization and data analysis.

### Analysis of serum markers and assessment of the immune organs index

On day 27 after induction, the blood, spleens and thymuses were collected from each group. Expression levels of the pro-inflammatory cytokines, TNF- $\alpha$  and IL-1 $\beta$ , in serum were measured using ELISA kits according to the standard protocol. Serum levels of aspartate aminotransferase (AST) and alanine transaminase (ALT) were measured using an automatic biochemical analyzer.

Spleens and thymuses collected from rats were accurately weighed to calculate the spleen and thymus index according to the following formula:

$$\text{Spleen index (\%)} = (\text{Spleen weight}) / (\text{Body weight}) \times 100\%$$

$$\text{Thymus Index (\%)} = (\text{Thymus weight}) / (\text{Body weight}) \times 100\%.$$

### Joint tissue histological evaluation

The ankle joints were decalcified in a neutral calcium EDTA decalcifying solution (14%) for 4-6 days until the joint tissue became soft with barbless resistance after complete decalcification. The decalcified ankle joints were bisected longitudinally on the median axis and paraffin-embedded by standard histological methods. Tissue sections (5  $\mu$ m) were processed and H&E stained for histological evaluation by a pathologist, who was blinded to the treatments.

Pathological changes were evaluated with modification of the previously described semi-quantitative scoring system for experimental arthritis in rats [31] as follows: synovial cell proliferation (0-2 points), pannus formation (0-3 points), mononuclear cell infiltration (0-3 points), infiltration of neutrophils in soft tissues around the joints (0-3 points), cell infiltration and distal tibia bone destruction (0-3 points), and chondrocyte infiltration (0-2 points). The H&E score of an ankle joint is the sum of histopathological features scores.

### Statistical analysis

Results were scored as the mean  $\pm$  standard deviation (SD) and analyzed using GraphPad Prism 6.0 (GraphPad Software, La Jolla, CA, USA). Statistical

comparisons were made to assess the difference between various groups using one-way analysis of variance (ANOVA). A *P* value less than 0.05 was considered statistically significant.

## Results

### Synthesis and structure identification of RGD-PEG<sub>3400</sub>-PLA<sub>2000</sub>

<sup>1</sup>H NMR was utilized to determine the formation of RGD-PEG<sub>3400</sub>-PLA<sub>2000</sub>. As shown in **Figure 1B**, the peak at 5.21 ppm corresponds to the tertiary PLA proton (m, -CH), and that at 3.62 ppm represents the protons of the repeating units in the PEG chain (m, OCH<sub>2</sub>-CH<sub>2</sub>O). The peak of 1.51 ppm is for the pend methyl group of PLA chain (m, -CH<sub>3</sub>). The chemical shift at 8.32 ppm is assigned to the H protons in RGD blocks.

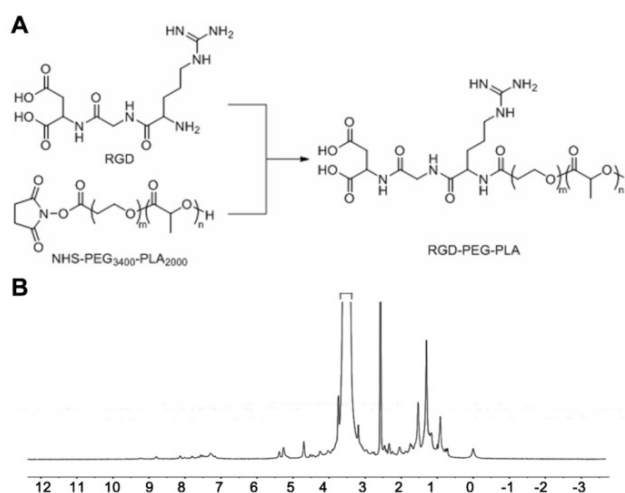


**Figure 1.** Synthesis and <sup>1</sup>H NMR spectrum of RGD-PEG<sub>3400</sub>-PLA<sub>2000</sub>. (A) NHS-PEG<sub>3400</sub>-PLA<sub>2000</sub> was reacted with RGD in anhydrous N, N-dimethyl formamide (DMF) containing triethylamine (TEA), with 1: 1.2: 1.2 molar ratio of NHS-PEG<sub>3400</sub>-PLA<sub>2000</sub>, RGD, and TEA. The mixture was stirred at room temperature for 24 h. (B) <sup>1</sup>H NMR (DMSO-d<sub>6</sub>) spectrum was used to identify the synthesized polymers.

### Characterization of particle size, zeta potential, and morphology of micelles

Based on DLS detection, the micelles showed small size and narrow size distribution (**Table 1**). The particle size of blank micelles (PMs) was 29.70  $\pm$  0.58 nm with a PDI of 0.17  $\pm$  0.04. After drug loading, it increased to 32.30  $\pm$  0.86 nm and 59.70  $\pm$  6.10 nm for MTX-PMs and NIM-PMs, respectively, and the particle sizes of R-MTX-PMs and R-NIM-PMs were 34.30  $\pm$  0.61 nm and 60.20  $\pm$  3.21 nm, respectively. Thus, there was no significant difference in the particle sizes between MTX-PMs *vs.* R-MTX-PMs and NIM-PMs *vs.* R-NIM-PMs (*P* > 0.05). The PDI data showed the uniformity of all particles and the zeta potential data indicated that all micelles had a neutral charge.

**Table 1.** Characteristics of micelles: size distribution, zeta potential, drug loading, and encapsulation efficiency.

Micelles	Particle Size (nm)	PDI	Zeta Potential (mV)	Drug Loading	Encapsulation Efficiency
PMs	29.70 ± 0.58	0.171 ± 0.04	0.00 ± 1.53	-	-
MTX-PMs	32.30 ± 0.86	0.236 ± 0.10	1.57 ± 0.06	4.97 ± 0.86	84.60 ± 9.51
R-MTX-PMs	34.30 ± 0.61	0.238 ± 0.21	1.60 ± 0.06	5.03 ± 0.67	85.36 ± 6.56
NIM-PMs	59.70 ± 6.10	0.321 ± 0.04	1.57 ± 2.14	5.67 ± 0.25	89.06 ± 8.58
R-NIM-PMs	60.20 ± 3.21	0.319 ± 0.07	1.60 ± 1.98	5.78 ± 0.32	90.78 ± 7.85

Abbreviation: PDI, polydispersity index. Results are expressed as mean ± SD from three independent experiments.

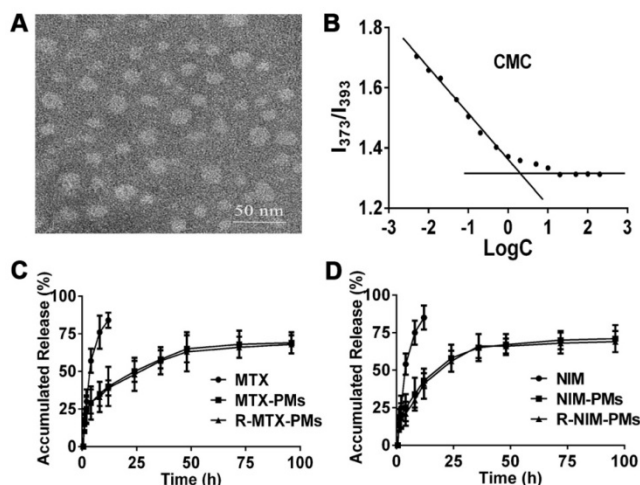


**Figure 2.** Characterization of micelles. (A) Morphology of blank micelles detected by transmission electron microscopy (TEM), bar = 50 nm. (B) Critical micelle concentration (CMC) of polymeric micelles. *In vitro* release profile of (C) MTX and (D) NIM in PBS containing 1% Tween-80. Results are presented as mean ± SD (n = 3).

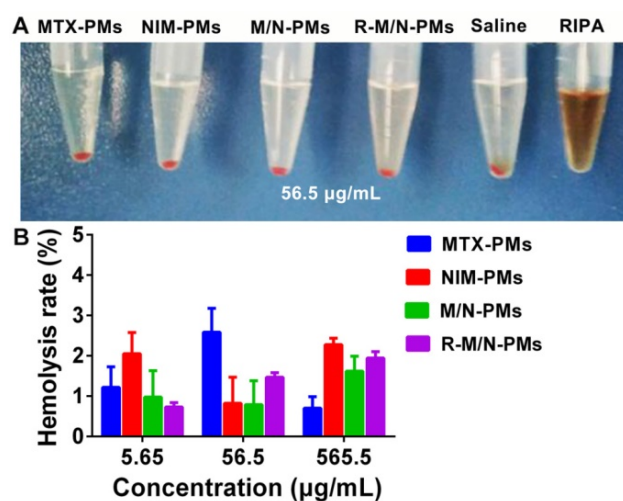


**Figure 3.** Hemolytic activity of micelles. (A) Red blood cells from healthy SD rats were incubated at 37 °C with different micelle formulations of MTX-PMs, NIM-PMs, M/N-PMs, and R-M/N-PMs with saline as negative and RIPA as positive controls. (B) Hemolytic activity of increasing concentrations of various micelle formulations

MTX and NIM were incorporated into the PEG<sub>3400</sub>-PLA<sub>2000</sub> micelles to form R-MTX-PMs and R-NIM-PMs with an encapsulation efficiency of 85.36 ± 6.56% and 90.78 ± 7.85% and drug loading yield of 5.03 ± 0.67% and 5.78 ± 0.32%, respectively. TEM demonstrated micelles with a uniform spherical shape

and an average size of about 30 nm (Figure 2A). This result was consistent with that obtained from the dynamic light scattering.

CMC was estimated to be 2.51 × 10<sup>-3</sup> mg/mL through the fluorescence method taking pyrene as a probe (Figure 2B). The *in vitro* release profile of MTX-PMs, NIM-PMs, R-MTX-PMs and R-NIM-PMs are shown in Figure 2C-D. All micelles formulations exhibited a sustained release profile compared to free MTX and NIM, in which both free drugs were released rapidly with up to about 85% cumulative release over the first 24 h. In contrast, only about 60% of MTX and 65% of NIM were released from drug-loaded micelles after 96 h. These results suggested that the micelle formulations of MTX-PMs, NIM-PMs, R-MTX-PMs, and R-NIM-PMs showed the advantage of controlled release at 37 °C in neutral medium.

### Analysis of hemolytic activity of micelles

Since the micelles are intended for the *in vivo* study, we first evaluated their biocompatibility by using the *in vitro* hemolysis test. As shown in Figure 3A, the positive control of RIPA induced massive hemolysis, while the micelle samples including MTX-PMs, NIM-PMs, M/N-PMs, and R-M/N-PMs induced erythrocyte lysis at a level similar to the negative control. Figure 3B shows that even at a concentration of up to 565 µg/mL, no obvious hemolytic activity was observed by any of the micelle samples with an average hemolysis rate of less than 3%. Therefore, these results demonstrated good biocompatibility of all four micelle formulations, MTX-PMs, NIM-PMs, M/N-PMs, and R-M/N-PMs.

### Effect of micelles on angiogenesis

To verify whether the micelle formulations could suppress angiogenesis, we used the CAM *in vivo* angiogenesis model in this study. As shown in Figure 4, compared to the saline group, the newly formed blood vessel branch points were decreased in the groups treated with MTX-PMs, NIM-PMs, M/N-PMs, R-MTX-PMs, R-NIM-PMs, and R-M/N-PMs, whereas in the PMs group they remained at the normal level. Among all micelle formulations, R-M/N-PMs showed the most potent inhibitory effect on angiogenesis of chick embryos in the CAM assay.

### Retention of R-M/N-PMs in arthritic joints

Real-time fluorescence imaging analysis revealed that systemically administered M/N-PMs-DiD or R-M/N-PMs-DiD mainly accumulated in arthritic joints (Figure 5A). The fluorescence signal was negligible in the limbs of arthritic rats receiving free DiD, but intense fluorescence in arthritic joints was detected as early as at 3 h post-injection and

lasted for more than 24 h. R-M/N-PMs-DiD showed stronger fluorescence signal in arthritic joints compared with M/N-PMs-DiD. To further investigate the biodistribution of R-M/N-PMs, the semi-quantitative analysis of fluorescence signal was carried out (Figure 5B). The graph illustrated a similar pattern as fluorescence images. These results suggested that R-M/N-PMs-DiD persisted longer in circulation and accumulated selectively in arthritic joints and that RGD enhanced the targeting ability of micelles and promoted their retention in arthritic joints. This is consistent with the result from the tissue biodistribution detection shown in Figure S4.

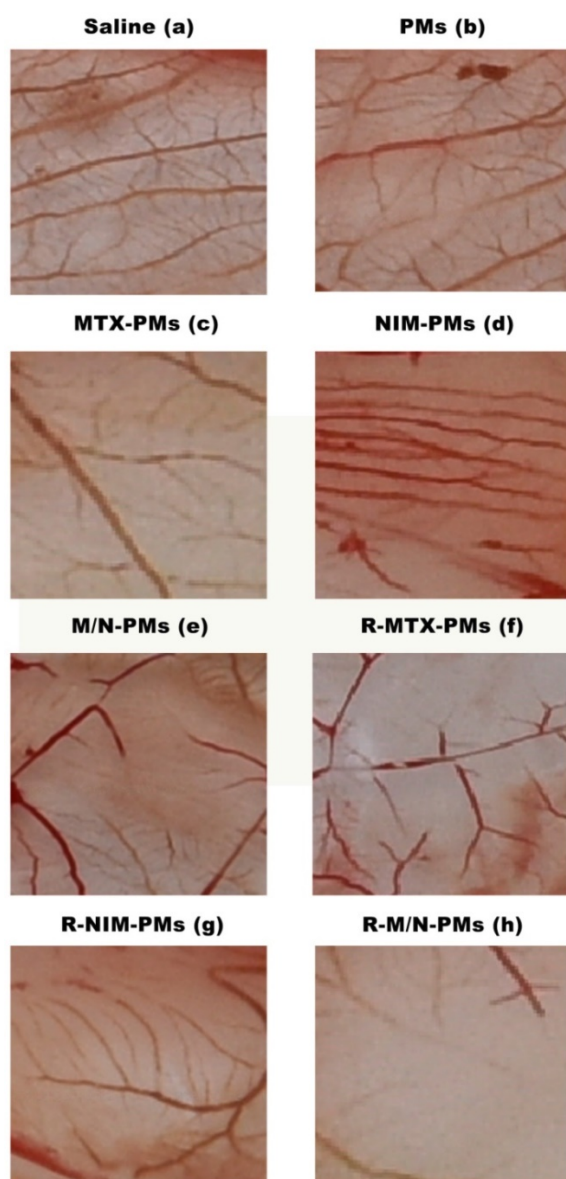


**Figure 4.** Inhibitory effects of micelle formulations on neovascularization in chick embryos. The CAM assay was performed as described in M&M section. Compared to the Saline control and the group treated with PMs, all other formulations showed a decrease in blood vessel branch points with the most significant decrease with R-M/N-PMs.

### Sustained amelioration of joint inflammation by R-M/N-PMs in arthritic rats

Mild swelling and erythema were observed on day 15 after CFA injection. On day 19, arthritis was fully developed when severe swelling and erythema appeared in the hind limbs and moderate symptoms in the front paws. Various micelle formulations were injected via the tail vein and then the ankle joint diameter and the joint index score were measured 5 times every other day. As shown in Figure 6A, arthritis progression appeared significantly different between different treatment groups after the 5th drug administration on day 27, which was visible by macroscopic examination.

In terms of the weight changes, compared to the saline control group, there was a continuous and pronounced increase from day 19 to 27 post-arthritis induction in the R-M/N-PMs group ( $p < 0.01$ ) (Figure 6B). Both saline and PMs groups showed a slight weight increase in rats whereas a moderate increase was observed in other groups.

The drug-loaded micelle formulations including MTX-PMs, NIM-PMs, M/N-PMs, R-MTX-PMs, R-NIM-PMs, and R-M/N-PMs resulted in a greater decrease in both ankle swelling (Figure 6C) and AI scores (Figure 6D) from day 19 to 27 post-arthritis induction, showing slower disease progression than saline and PMs. The ankle diameter of the R-M/N-PMs group appeared to be significantly lower ( $P < 0.05$ ) than the other micelle-treated groups and saline group; but was significantly higher ( $P < 0.05$ ) than the normal healthy control. No significant differences were observed between PMs and saline groups ( $P > 0.05$ ).

### Impact of micelles on the bone microstructure and serum biochemical markers

Figure 7A shows the three-dimensional reconstruction images of the bone microstructure obtained from micro-CT. The quantitative analysis of bone mineral density (BMD) is presented in Figure 7B. From these images and BMD data, it is evident that severe bone damage occurred in the saline and PMs groups with extensive erosion of the entire tibia. Compared to the saline group, MTX-PMs- and R-MTX-PMs-treated animals demonstrated a moderate erosion of the ankle bone ( $P < 0.05$ ); M/N-PMs and R-M/N-PMs significantly helped to recover bone microstructure with minor erosion ( $P < 0.01$ ).

It has been reported that IL-1 $\beta$  and TNF- $\alpha$  are the most important pro-inflammatory cytokines involved in the progression of joint synovial damage in RA [32, 33]. Following arthritis induction, both IL-1 $\beta$  and TNF- $\alpha$  increased significantly compared to the healthy controls (Figure 7C-D). The increased levels

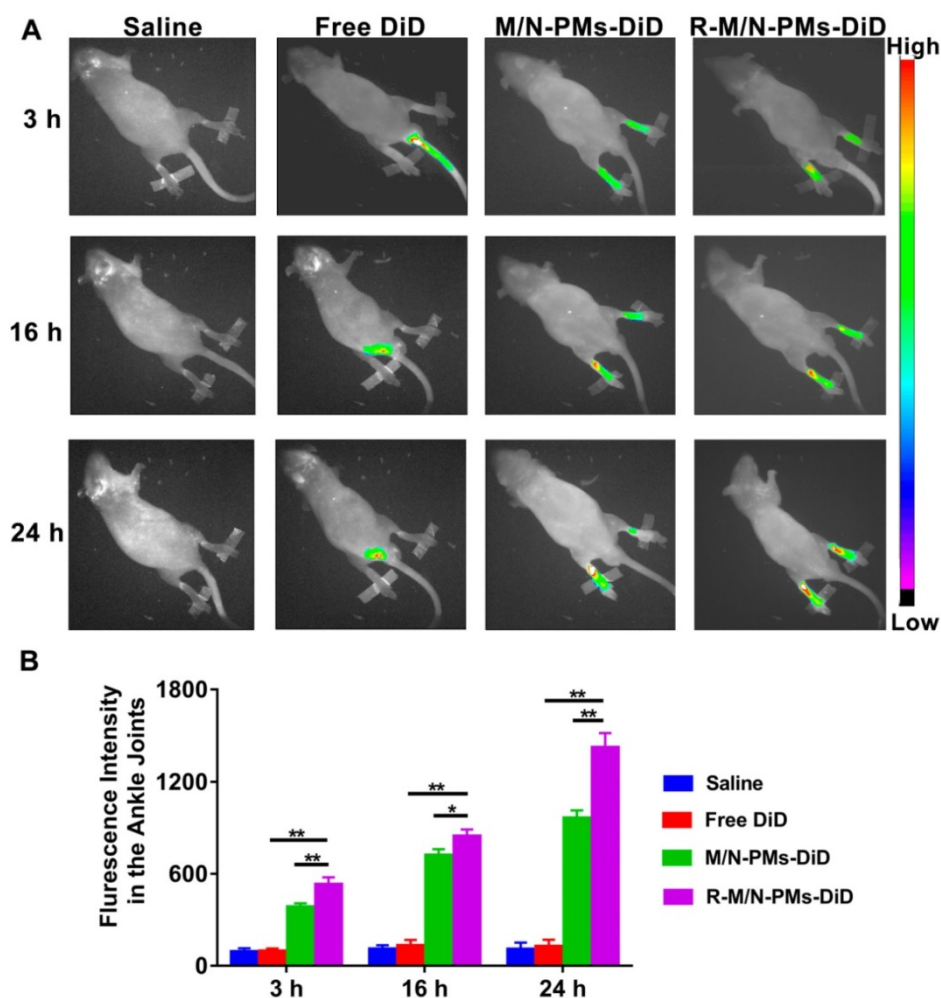


**Figure 5.** *In vivo* distributions of micelles in arthritic rats (A) and average fluorescence intensity detected from ankle joints (B). The arthritic rats received an intravenous injection of free DiD, M/N-PMs-DiD, R-M/N-PMs-DiD, and saline as control. Data were presented as mean  $\pm$  SD (n = 3; \*P < 0.05, \*\*P < 0.01).

of IL-1 $\beta$  and TNF- $\alpha$  were maintained after treatment with saline and PMs, whereas treatment with NIM-PMs resulted in a slight decrease and with MTX-PMs, R-MTX-PMs and R-NIM-PMs led to a moderate decrease in both cytokines (P < 0.05). However, both M/N-PMs and R-M/N-PMs significantly decreased the expression levels of IL-1 $\beta$  and TNF- $\alpha$  (P < 0.01), with R-M/N-PMs leading to a greater decrease.

In the normal controls, the serum levels of ALT were similar to those in animals treated with saline and micelle formulations (Figure 7E). But arthritis progression increased the AST level (Figure 7F) that was maintained after treatment with saline or PMs. Compared to saline or PMs group, treatment with other drug-loaded micelles resulted in a pronounced reduction of AST (P < 0.05, P < 0.01). This result indicated that the targeted delivery of R-M/N-PMs likely help to reduce the liver toxicity in the arthritic rats.

RA is an immune disease, so an index of the immune organs could reflect the disease progression

to a certain extent. As shown in Table 2, both spleen and thymus indices of arthritic rats treated with saline and PMs were significantly higher than that of the healthy controls. Compared to the saline group, M/N-PMs and R-M/N-PMs remarkably reduced the indices of spleen and thymus (P < 0.01) reaching almost the normal levels.

**Table 2.** Spleen and thymus index of rats post-treatment with various micelle formulations

Groups	Dosage (mg/kg)	Spleen index (%)	Thymus index (%)
Normal	-	0.198 $\pm$ 0.013	0.134 $\pm$ 0.023
Saline	-	0.293 $\pm$ 0.028	0.169 $\pm$ 0.018
PMs	3.0	0.283 $\pm$ 0.019	0.163 $\pm$ 0.017
MTX-PMs	0.6	0.234 $\pm$ 0.025	0.150 $\pm$ 0.023
NIM-PMs	3.0	0.250 $\pm$ 0.027	0.152 $\pm$ 0.025
M/N-PMs	0.6MTX + 3.0NIM	0.211 $\pm$ 0.019**	0.142 $\pm$ 0.017**
R-MTX-PMs	0.6	0.216 $\pm$ 0.031*	0.151 $\pm$ 0.029
R-NIM-PMs	3.0	0.218 $\pm$ 0.033*	0.154 $\pm$ 0.012
R-M/N-PMs	0.6MTX + 3.0NIM	0.210 $\pm$ 0.016**	0.140 $\pm$ 0.014**

Results are presented as mean  $\pm$  S.D. (n=5). Symbols represent statistical significance compared with the control group (\*P < 0.05, \*\*P < 0.01).

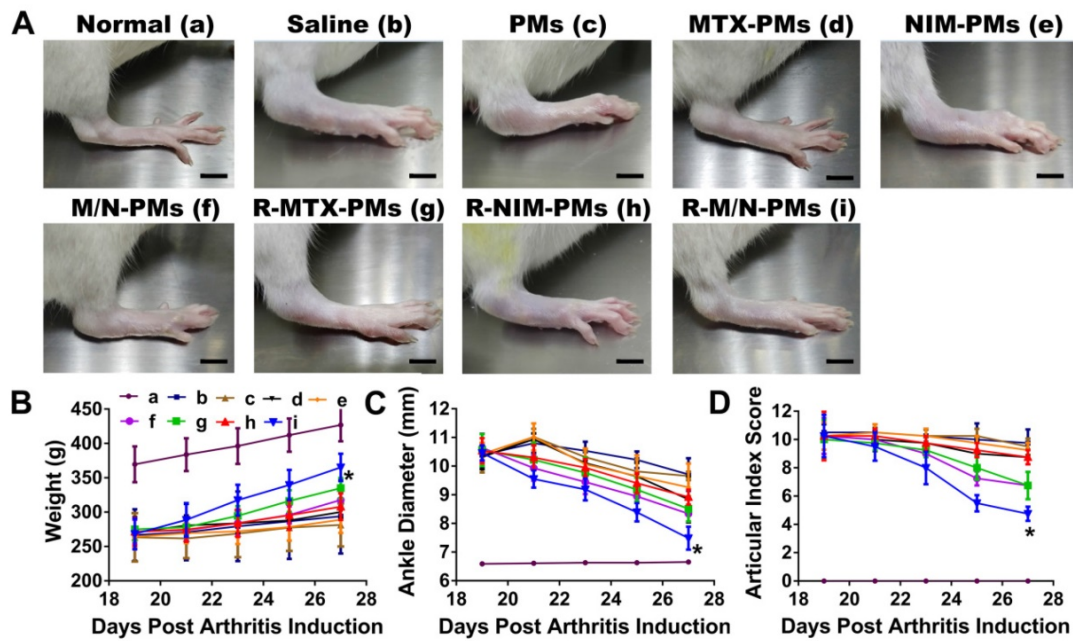


**Figure 6.** *In vivo* therapeutic effects of micelles in rats with adjuvant-induced arthritis. On day 19 post-induction, the rats with established arthritis were given different micelle formulations every other day for 4 times. (A). Representative photographs of hind legs were taken on the 27<sup>th</sup> day (B), weight, (C) ankle diameter, and (D) articular index scores show the strongest effect of the R-M/N-PMs micelles. Results are shown as mean  $\pm$  SD (n=5). Symbols P represented statistical significance with \*P < 0.050. The bar is 75 mm.

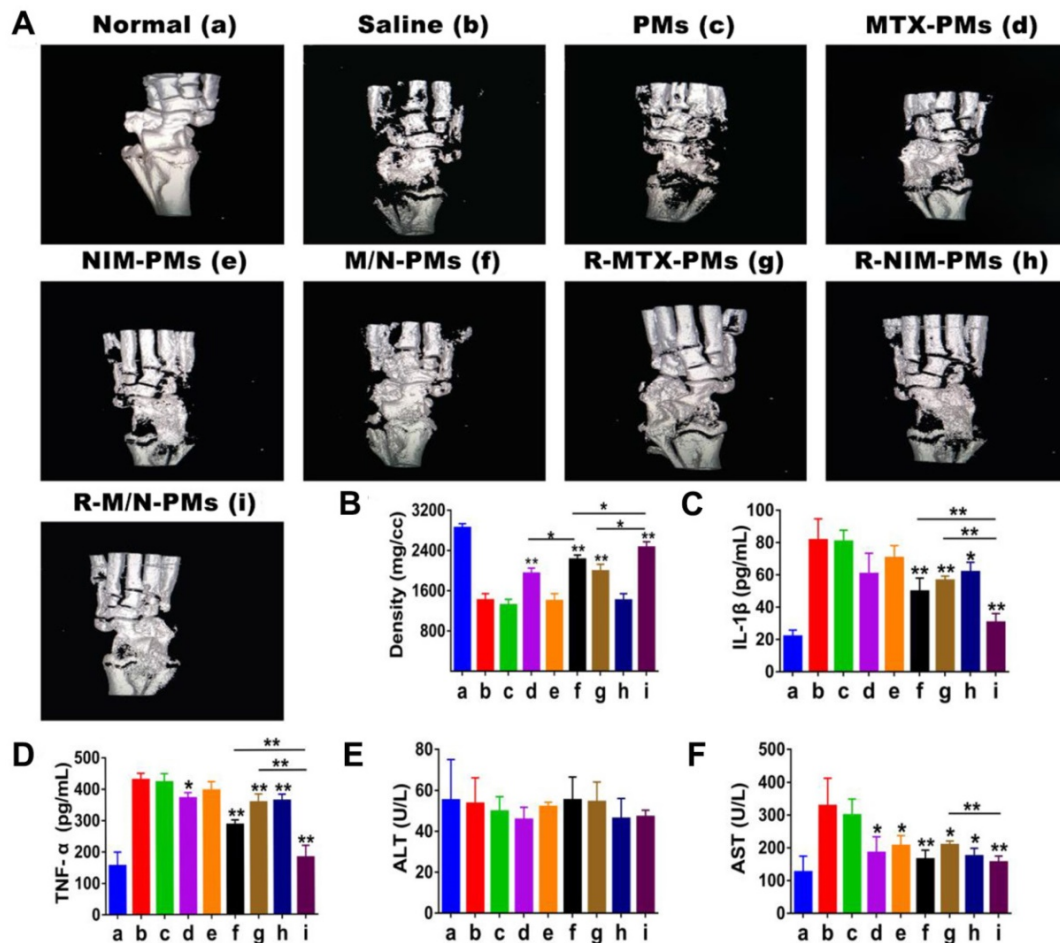


**Figure 7.** Impact of micelles on the bone microstructure and serum biomarkers. (A) Significant restoration of the bone microarchitecture analyzed by micro CT on day 27 after induction and (B) Quantitative analysis of bone mineral density. The maximum effect was observed in both parameters by R-M/N-PMs. Serum biomarkers of (C) IL-1 $\beta$  and (D) TNF- $\alpha$  analyzed by ELISA; that of (E) ALT and (F) AST measured using an automatic biochemical analyzer. Results are shown as mean  $\pm$  SD (n=4). Symbols P represented statistical significance with \*P < 0.05 and \*\*P < 0.01.

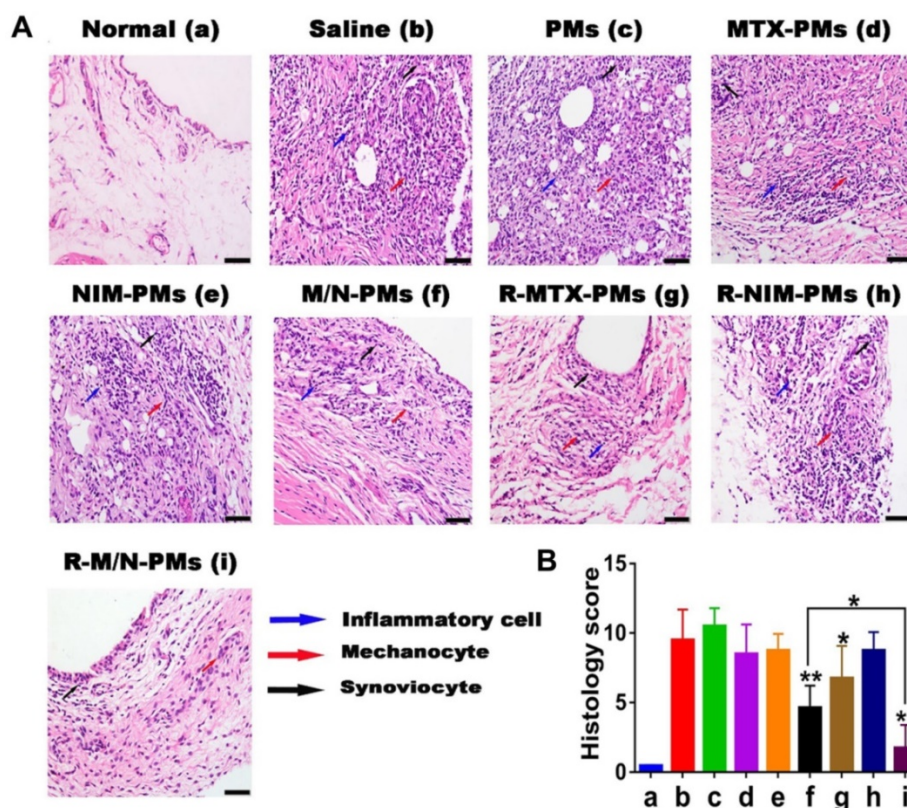


**Figure 8.** Histopathology analysis of the ankle joint. (A) H&E staining. The inflammatory cells, melanocytes, and synoviocyte are marked by bold blue, red, and black arrows, respectively. The bar is 100  $\mu$ m. (B) Histopathology scores. Results are shown as mean  $\pm$  SD (n=5). Symbols P represented statistical significance with \* $P < 0.05$  and \*\* $P < 0.01$ .

### Histological analysis of ankle joints

Representative images from the tissue histopathology analyses of the ankle joints isolated at the end point of the *in vivo* experiment are shown in **Figure 8A**. Compared to healthy control animals, histological analysis revealed marked periosteal expansion, inflammatory cell infiltration, pannus formation, and distal tibia bone destruction in saline- and PMs-treated groups. However, the treatment groups of M/N-PMs and R-M/N-PMs displayed markedly reduced joint damage and cellular infiltration with bone and cartilage morphology maintained at a level similar to that of the healthy rats. The sum of the score from each animal was recorded and is shown in **Figure 8B**. A statistically significant difference was found between saline *vs.* other groups, M/N-PMs ( $P < 0.01$ ), R-MTX-PMs ( $P < 0.05$ ), and R-M/N-PMs ( $P < 0.01$ ) as well as M/N-PMs *vs.* R-M/N-PMs ( $P < 0.05$ ) groups. No significant difference was found between saline and PMs.

### Discussion

Angiogenesis plays an important role in the progression of RA, which is considered an angiogenesis-dependent disease [34]. We conducted this study to evaluate whether the combination of methotrexate and nimesulide mediated by

RGD-modified polymeric micelles, R-M/N-PMs, could target and inhibit angiogenesis and thus enhance the therapeutic effect of drugs on rheumatoid arthritis. We successfully synthesized RGD-functionalized polymers, RGD-PEG<sub>3400</sub>-PLA<sub>2000</sub>, to formulate RGD-modified drug-loaded micelles by the thin-film hydration method. R-M/N-PMs not only significantly inhibited the viability of the inflammatory RAW264.7 cells but also markedly suppressed angiogenesis of chick embryos in the CAM assay. We further conducted the real-time fluorescence imaging analyses using the *in vivo* small animal imaging system and observed that systemically administered R-M/N-PMs labeled by DiD mainly distributed to arthritic joints and that RGD enhanced the targeting ability of micelles and thus promoted the retention of micelles in arthritic joints. Most importantly, the *in vivo* study of the arthritic rats demonstrated that R-M/N-PMs reduced the joint swelling, immune organs index, bone erosion, and serum levels of inflammatory cytokines and thus enhanced the therapeutic efficacy for rheumatoid arthritis.

The particle size of the polymeric micelles was between 25 nm and 65 nm suitable for tail vein injection in rats. However, the zeta potential indicated that the micelles had a neutral charge. Zeta potential and CMC of micelles are the two important characteristics that determine the stability of micelles.

In general, a high absolute value of zeta potential contributes to the better dynamic stability of the micelles [35]. However, the zeta potential value of the polymeric micelles prepared in this study indicated that they might be unstable, but the CMC determination suggested reasonable stability. We, therefore, conducted the stability experiment and found that the micelle solution, when stored at 4 °C, showed no changes for 30 days with an average drug-leakage rate of about 1% (data not shown). This stability may be due to the high content of PEG on the micelle surface providing a repulsive force to reduce the surface tension between particles and thus help maintain the stability. This observation is consistent with a previous published report [36, 37].

The RGD peptide is a specific ligand for  $\alpha_v\beta_3$ -integrin expressed on endothelial cells at sites of inflammation [38]. In our study, the *in vitro* cell viability assay indicated that RGD-containing micelles significantly enhanced the inhibition effect on cell-growth of LPS-stimulated Raw264.7 cells compared to the RGD-free micelles demonstrating the significance of RGD in the therapy of inflammation-related diseases. In the *in vivo* assay of arthritic rat model, both R-M/N-PMs and M/N-PMs, when intravenously injected, mainly distributed to the arthritic joints. This may be due to the passive targeting of micelles to the inflammation sites through the ELVIS mechanism (Extravasation through Leaky Vasculature and Inflammatory cell-mediated Sequestration) in which, after systemic administration, both R-M/N-PMs and M/N-PMs could pass through the leaky vasculature of inflammatory lesions and internalize into the inflammatory infiltrates and locally activated resident cells [39]. However, at 24 h post-injection, the R-M/N-PMs group maintained stronger fluorescence signal than the M/N-PMs group because of the high affinity and selectivity of RGD with integrin  $\alpha_v\beta_3$  thus promoting the retention of micelles in arthritic joints.

The CAM assay is often used to study tumor angiogenesis [40]. Since the angiogenesis in rheumatoid arthritis is similar to that in tumors [41], we used this assay to investigate whether the micelle formulations could inhibit angiogenesis. Methotrexate is a cytotoxic drug and therefore MTX-PMs showed a stronger inhibitory effect on neovascularization than NIM-PMs with nimesulide, an anti-inflammatory drug. In the R-M/N-PMs group, the combination of methotrexate and nimesulide together with the RGD's specificity for the integrin receptor over-expressed in neovascular endothelial cells resulted in the most significant inhibition effect among all the micelle formulations.

*In vivo* toxicity problems of nano-drug delivery systems, such as liver toxicity, blood compatibility, immunogenicity and myelo-suppression, have been one of the main factors limiting their clinical application. As shown in the supplementary file (Figure S4), the major organs for nano-sized micelles to reach in the healthy are liver and spleen, which is consistent with the other report [42]. But in the arthritic rats, micelles mainly accumulated on ankle joints. This may be one of the reasons that the targeted delivery of R-M/N-PMs was found to help reduce systemic toxicity in the arthritic rats, which suggested by the result from the blood levels of ALT and AST.

It has been reported that the use of NSAIDs partially alleviates the symptoms of rheumatoid arthritis but cannot prevent its long-term disease progression [43]. Therefore, nimesulide did not lead to a significant difference between the R-NIM-PMs group and the saline group in the histopathology score of the ankle joint. However, Al-Abd et al. reported that nimesulide improved the anti-rheumatic profile of methotrexate in the collagen-induced arthritic mice model [13]. In our present study, we found that the combination therapy of methotrexate and nimesulide mediated by RGD-modified polymeric micelles enhanced the therapeutic efficacy in rheumatoid arthritis. However, in our study, we formulated methotrexate and nimesulide separately into the polymeric micelles. The rats with arthritis were given methotrexate (0.6 mg/kg) and nimesulide (3.0 mg/kg) as micelle formulations by intravenous injection every other day, in which not only the dose of both methotrexate and nimesulide was significantly decreased but also the simple administration method of 'same time and same injection' provided a more convenient procedure for the potential clinical application.

In summary, the combination therapy of methotrexate and nimesulide mediated by RGD-modified polymeric micelles showed promising results in the rat model of rheumatoid arthritis. However, rheumatoid arthritis is a chronic autoimmune disease and the animal models of rheumatoid arthritis can be affected by multiple factors, such as animal strains, feeding environment, and concentration of Mycobacterium tuberculosis. Although the animal model of rheumatoid arthritis used in this study is very similar to the human rheumatoid arthritis in terms of its pathological features, it lacks the chronic course of the human disease. Therefore, in the future, it is necessary to study other animal models that more closely mimic the human disease to obtain more useful information for the clinical therapy of rheumatoid arthritis.

## Conclusion

We successfully developed a novel targeted drug delivery system, RGD-modified polymeric micelles loaded with low-doses of methotrexate and nimesulide in a fixed dose combination, which significantly enhanced the therapeutic effect on rheumatoid arthritis. Our strategy holds great promise for future clinical applications to alleviate a common debilitating human ailment.

## Abbreviations

AST: aspartate aminotransferase; ALT: alanine transaminase; AI: articular index; CFA: complete Freund's adjuvant; CMC: critical micelle concentration; CAM: chick chorioallantoic membrane; DMEM: Dulbecco's modified eagle's medium; DMSO: dimethyl sulfoxide; DMF: N,N-dimethyl formamide; DLS: dynamic light scattering; DL: drug loading; EE: encapsulation efficiency; FBS: fetal bovine serum; HPLC: high-performance liquid chromatography; H&E: hematoxylin-eosin staining; HUVEC: human umbilical vein endothelial cell line; LPS: lipopolysaccharide; MTX: methotrexate; Micro-CT: micro-computed tomography; MTT: 3-(4,5-dimethylthiazol-2-yl)-2,5-diphenyl-tetrazolium bromide; NIM: nimesulide; RBCs: red blood cells; RA: rheumatoid arthritis; RIPA: ristocetin-induced platelet agglutination; SD: standard deviation; TEM: transmission electron microscopy; TEA: anhydrous triethylamine.

## Supplementary Material

Supplementary methods and figures.  
<http://www.thno.org/v09p0708s1.pdf>

## Acknowledgments

All authors are thankful for getting help and supports from the following research platforms of the Key Laboratory of Medical Electrophysiology of Ministry of Education, Collaborative Innovation Center for Prevention and Treatment of Cardiovascular Disease, the Drug Discovery Research Center, the Department of Medicinal Chemistry, School of Pharmacy, Southwest Medical University, Luzhou, Sichuan 646000, China.

## Funding

This work was supported by the General Program of Science and Technology Agency of Sichuan Province (2017JY0160, 2018RZ0120); the Collaborative Fund of Luzhou Government and Southwest Medical University (2016LZXNYD-J06 and 2017LZXNYD-T07); the Science and Technology Project of the Health Planning Committee of Sichuan

(18PJ547); the Key Science and Technology Project of Luzhou Government (2018-SYF-19); the Key Fund, the Youth Fund and the Transformation Project of Science and Technology Achievements of Southwest Medical University (2018-ZRZD-018, 2017-ZRQN-073, 2018002), the Opening Project of the Key Laboratory of Drug Targeting and Drug Delivery System of the Ministry of Education (Sichuan University), and the Collaborative Project of Luzhou TCM Hospital and Southwest Medical University (2017-LH004).

## Competing Interests

The authors have declared that no competing interest exists.

## References

- Hua S, Dias TH. Hypoxia-inducible factor (HIF) as a target for novel therapies in rheumatoid arthritis. *Front pharmacol.* 2016; 7: 184.
- Mateen S, Zafar A, Moin S, Khan AQ, Zubair S. Understanding the role of cytokines in the pathogenesis of rheumatoid arthritis. *Clin Chim Acta.* 2016; 455: 161-71.
- Mankia K, Emery P. Preclinical rheumatoid arthritis: progress toward prevention. *Arthritis Rheumatol.* 2016; 68: 779-88.
- Caramaschi P, Bambara LM, Pieropan S, Tinazzi I, Volpe A, Biasi D. Anti-TNFalpha blockers, autoantibodies and autoimmune diseases. *Joint Bone Spine.* 2009; 76: 333-42.
- Fehér J, Lengyel G. Effectiveness and safety of biological therapy with adalimumab. *Orv Hetil.* 2009; 150: 1215-22.
- Bracewell C, Isaacs JD, Emery P, Ng WF. Atacept, a novel B cell-targeting biological therapy for the treatment of rheumatoid arthritis. *Expert Opin Biol Ther.* 2009; 9: 909-19.
- Martinez Lopez JA, Loza E, Carmona L. Systematic review on the safety of methotrexate in rheumatoid arthritis regarding the reproductive system (fertility, pregnancy, and breastfeeding). *Clin Exp Rheumatol.* 2009; 27: 678-84.
- Ding H, Gao G, Zhang L, Shen G, Sun W, Gu Z, et al. The protective effects of curcuglucoside A on adjuvant-induced arthritis by inhibiting NF- $\kappa$ B, MyD88, and NLRP3 activation in rats. *Int Immunopharmacol.* 2016; 30: 43-9.
- Yang M, Ding J, Feng X, Chang F, Wang Y, Gao Z, et al. Scavenger receptor-mediated targeted treatment of collagen-induced arthritis by dextran sulfate-methotrexate prodrug. *Theranostics.* 2017; 7: 97-105.
- Yang M, Chang F, Ding J, Wang J, Gao Z, Zhuang X, et al. Scavenger receptor-targeted dextran sulfate-methotrexate prodrug for treatment of collagen-induced arthritis. *J Control Release.* 2017; 259: e98.
- Qi R, Majoros I, Misra AC, Koch AE, Campbell P, Marotte H, et al. Folate receptor-targeted dendrimer-methotrexate conjugate for inflammatory arthritis. *J Biomed Nanotechnol.* 2015; 11: 1431-41.
- Suleyman H, Cadirci E, Albayrak A, Halici Z. Nimesulide is a selective COX-2 inhibitor, atypical non-steroidal anti-inflammatory drug. *Curr Med Chem.* 2008; 15: 278-83.
- Al-Abd AM, Inglis JJ, Nofal SM, Khalifa AE, Williams RO, El-Eraky WI, et al. Nimesulide improves the disease modifying anti-rheumatic profile of methotrexate in mice with collagen-induced arthritis. *Eur J Pharmacol.* 2010; 644: 245-50.
- Yang M, Feng X, Ding J, Chang F, Chen X. Nanotherapeutics relieve rheumatoid arthritis. *J Control Release.* 2017; 252: 108-24.
- Yang M, Ding J, Zhang Y, Chang F, Wang J, Gao Z, et al. Activated macrophage-targeted dextran-methotrexate/folate conjugate prevents deterioration of collagen-induced arthritis in mice. *J Mater Chem B.* 2016; 4: 2102-13.
- Yang M, Chang F, Ding J, Gao Z, Zhuang X, Chen X. Treatment of collagen-induced arthritis by activated macrophage-targeted dextran-methotrexate/folate conjugate. *Nanomedicine.* 2018; 14: 1815-6.
- Feng XR, Ding JX, Gref R, Chen XS. Poly( $\beta$ -cyclodextrin)-mediated polylactide-cholesterol stereocomplex micelles for controlled drug delivery. *Chinese J Polym Sci.* 2017; 35: 693-9.
- Shen K, Li D, Guan J, Ding J, Wang Z, Gu J, et al. Targeted sustained delivery of antineoplastic agent with multicomponent polylactide stereocomplex micelle. *Nanomedicine.* 2017; 13:1279-88.
- Yuan F, Quan LD, Cui L, Goldring SR, Wang D. Development of macromolecular prodrug for rheumatoid arthritis. *Adv Drug Deliv Rev.* 2012; 64: 1205-19.
- Ferrari M, Onuoha SC, Pitzalis C. Going with the flow: harnessing the power of the vasculature for targeted therapy in rheumatoid arthritis. *Drug Discov Today.* 2016; 21: 172-9.
- Wang Y, Wang X, Zhang Y, Yang S, Wang J, Zhang X, et al. RGD-modified polymeric micelles as potential carriers for targeted delivery to

- integrin-overexpressing tumor vasculature and tumor cells. *J Drug Target.* 2009; 17: 459-67.
22. Zhang H, Xia H, Wang J, Li Y. High intensity focused ultrasound-responsive release behavior of PLA-b-PEG copolymer micelles. *J Control Release.* 2009; 139: 31-9.
23. Wei Z, Hao J, Yuan S, Li Y, Juan W, Sha X, et al. Paclitaxel-loaded pluronic P123/F127 mixed polymeric micelles: formulation, optimization and in vitro characterization. *Int J pharm.* 2009; 376: 176-85.
24. Basu Ray G, Chakraborty I, Moulik SP. Pyrene absorption can be a convenient method for probing critical micellar concentration (cmc) and indexing micellar polarity. *J Colloid Interf Sci.* 2006; 294: 248-54.
25. Jain A, Agarwal A, Majumder S, Lariya N, Khaya A, Agrawal H, et al. Mannosylated solid lipid nanoparticles as vectors for site-specific delivery of an anti-cancer drug. *J Control Release.* 2010; 148: 359-67.
26. Park BC, Park SY, Lee JS, Mousa SA, Kim JT, Kwak MK, et al. The anti-angiogenic effects of 1-furan-2-yl-3-pyridin-2-yl-propenone are mediated through the suppression of both VEGF production and VEGF-induced signaling. *Vasc Pharmacol.* 2009; 50: 123-31.
27. Kim BS, Park H, Ko SH, Lee WK, Kwon HJ. The sphingosine-1-phosphate derivative NHOBTD inhibits angiogenesis both in vitro and in vivo. *Biochem Bioph Res Co.* 2011; 413: 189-93.
28. Wang Q, Jiang J, Chen W, Jiang H, Zhang Z, Sun X. Targeted delivery of low-dose dexamethasone using PCL-PEG micelles for effective treatment of rheumatoid arthritis. *J Control Release.* 2016; 230: 64-72.
29. Zhang L, Cui M, Ding L, Xia L, Lu J, Shen H. Interleukin-34 aggravates the severity of arthritis in collagen-induced arthritis mice by inducing interleukin-17 production. *J Interferon Cytokine Res.* 2018; 38: 221-5.
30. Quan L, Zhang Y, Crielard BJ, Dusad A, Lele SM, Rijcken CJF, et al. Nanomedicines for inflammatory arthritis: head-to-head comparison of glucocorticoid-containing polymers, micelles, and liposomes. *ACS nano.* 2014; 8: 458-66.
31. Quan LD, Purdue PE, Liu XM, Boska MD, Lele SM, Thiele GM, et al. Development of a macromolecular prodrug for the treatment of inflammatory arthritis: mechanisms involved in arthrotropism and sustained therapeutic efficacy. *Arthritis Res Ther.* 2010; 12: R170.
32. Taylor PC, Williams RO. Combination cytokine blockade: the way forward in therapy for rheumatoid arthritis? *Arthritis Rheumatol.* 2015; 67: 14-6.
33. Reum Son A, Kim DY, Hun Park S, Yong Jang J, Kim K, Ju Kim B, et al. Direct chemotherapeutic dual drug delivery through intra-articular injection for synergistic enhancement of rheumatoid arthritis treatment. *Sci Rep.* 2015; 5: 14713.
34. Gayetskyy S, Museyko O, Kasser J, Hess A, Schett G, Engelke K. Characterization and quantification of angiogenesis in rheumatoid arthritis in a mouse model using  $\mu$ CT. *BMC Musculoskelet Disord.* 2014; 15: 298.
35. Wang H, Liu M, Du S. Optimization of madecassoside liposomes using response surface methodology and evaluation of its stability. *Int J Pharm.* 2014; 473: 280-5.
36. Bae Y, Alani AW, Rockich NC, Lai TS, Kwon GS. Mixed pH-sensitive polymeric micelles for combination drug delivery. *Pharm Res.* 2010; 27: 2421-32.
37. Wang J, Xu W, Li S, Qiu H, Li Z, Wang C, et al. Polylactide-cholesterol stereocomplex micelle encapsulating chemotherapeutic agent for improved antitumor efficacy and safety. *J Biomed Nanotechnol.* 2018; 14: 2102-13.
38. Chen H, Niu G, Wu H, Chen X. Clinical application of radiolabeled RGD peptides for PET imaging of integrin  $\alpha$ v $\beta$ 3. *Theranostics.* 2016; 6: 78-92.
39. Quan L, Zhang Y, Dusad A, Ren K, Purdue PE, Goldring SR, et al. The evaluation of the therapeutic efficacy and side effects of a macromolecular dexamethasone prodrug in the collagen-induced arthritis mouse model. *Pharm Res.* 2016; 33: 186-93.
40. Liu M, Scanlon CS, Banerjee R, Russo N, Inglehart RC, Willis AL, et al. The histone methyltransferase EZH2 mediates tumor progression on the chick chorioallantoic membrane assay, a novel model of head and neck squamous cell carcinoma. *Transl Oncol.* 2013; 6: 273-81.
41. Lupia E, Montrucchio G, Battaglia E, Modena V, Camussi G. Role of tumor necrosis factor- $\alpha$  and platelet-activating factor in neoangiogenesis induced by synovial fluids of patients with rheumatoid arthritis. *Eur J Immunol.* 1996; 26: 1690-4.
42. Blanco E, Shen H, Ferrari M. Principles of nanoparticle design for overcoming biological barriers to drug delivery. *Nat Biotechnol.* 2015; 33: 941-51
43. Weinblatt ME. Rheumatoid arthritis: treat now, not later! *Ann Intern Med.* 1996; 124: 773-4.